Available online at www.sciencedirect.com

ScienceDirect

Ceramics International 40 (2014) 2619–2625

CERAMICS INTERNATIONAL

www.elsevier.com/locate/ceramint

Visible-light photocatalytic activity of SiC hollow spheres prepared by a vapor–solid reaction of carbon spheres and silicon monoxide

Ouyang Haibo[a,*], Huang Jianfeng[a], Zeng Xierong[b,c], Cao Liyun[a], Li Cuiyan[a], Xiong Xinbo[b,c], Fei Jie[a]

[a]College of Materials Science & Technology, Shaanxi University of Science & Technology, Xi'an, Shaanxi 710021, China
[b]College of Materials Science & Engineering, Shenzhen University, Shenzhen 518060, China
[c]Shenzhen Key Laboratory of Special functional Materials, Shenzhen 518060, China

Received 5 September 2013; received in revised form 18 October 2013; accepted 18 October 2013
Available online 26 October 2013

Abstract

SiC hollow spheres are obtained by a vapor–solid reaction using carbon spheres as templates. The prepared SiC hollow spheres are characterized by X-ray diffraction, scanning electron microscopy, nitrogen adsorption, and UV–vis diffuse reflectance spectra. The visible-light photocatalytic activity is evaluated by photocatalytic decomposition of the methylene blue in aqueous solution. Results show that the diameter of SiC hollow spheres ranges from 200 to 300 nm and the shell thickness is about 50 nm. The SiC hollow spheres have a high surface area of 83.5 m^2/g and exhibit a mesoporous structure characteristic. The photo-response of the SiC hollow spheres expand to visible-light region with band gap energy of 2.15 eV. The SiC hollow spheres exhibit a significantly enhanced photocatalytic activity due to their high surface area as well as large light-harvesting efficiencies.

Keywords: D. SiC; Hollow spheres; Photocatalytic activity; Absorption

1. Introduction

Photocatalysis is a rapidly developing research field with a high potential for industrial applications, including mineralization of organic pollutants, disinfection of water and air, production of renewable fuels, and organic syntheses [1,2]. Today, semiconductor photocatalysis has emerged as one of the most promising technologies to utilize the energy of either natural sunlight or artificial indoor illumination [3,4]. Among the possible semiconductors, SiC is considered as a potential photocatalystic materials. SiC is one of the third-generation semiconductor materials with suitable band gap (2.3–3.3 eV) and excellent properties, such as high thermal conductivity, high mechanical strength, and high chemical stability, which make it a very promising photocatalyst under visible-light irradiation [5–7].

Nanostructured SiC, because of its low dimensionality, quantum confinement and shape effect, possesses even more promising mechanical, electronic and optical properties [8–10]. Recently, the photocatalysis of nanostructured SiC materials has received considerable attentions. Zhou et al. [11] reported that SiC nanowires exhibit an excellent photocatalytic activity for the decomposition of gaseous acetaldehyde. Liu et al. [12] reported that the porous SiC nanowire arrays showed good photoelectrochemical hydrogen evolution performance under UV irradiation. Ultrathin 3C–SiC nanocrystals with surface autocatalytic effects were possessing high efficiency electrochemical hydrogen evolution performance [13]. β-SiC nanowires can absorb visible-light and exhibit excellent photocatalytic hydrogen evolution performance from pure water under visible-light irradiation [14].

Nowadays, hollow sphere structures are of great interest in the field of photocatalysis, due to the lower density, monodisperse, high active area for catalysis and adsorption, and good ability to withstand cyclic changes in volume [15–17]. Thus, SiC hollow spheres are a candidate for photocatalytic

*Corresponding author. Tel./fax: +86 298 616 8802.
E-mail addresses: huangjf@sust.educn, ouyangsust@126.com (O. Haibo), licuiyan@sust.edu.cn (L. Cuiyan).

0272-8842/$ - see front matter © 2013 Elsevier Ltd and Techna Group S.r.l. All rights reserved.
http://dx.doi.org/10.1016/j.ceramint.2013.10.068

application. Liu et al. [18] prepared the SiC hollow spherical nanocrystals using a vapor–solid reaction between carbon nanoparticles and silicon monoxide vapor generated from a mixture of silicon and silica. Wang et al. [19] fabricated SiC hollow spheres from a mesoporous SiO_2–C nanocomposite. Li et al. [20] prepared SiC hollow nanospheres by a metal coreduction route. However, there are few reports about the photocatalytic of SiC with hollow spherical morphology.

In this work, SiC hollow spheres were fabricated by a vapor–solid reaction between carbon spheres and silicon monoxide vapor. The phase composition, morphology, microstructure, and surface area of the prepared SiC hollow spheres are characterized. The aim of this research is to investigate the photocatalytic properties of the SiC hollow spheres under visible-light irradiation.

2. Material and methods

2.1. Preparation of carbon spheres

Glucose was employed as the carbon source for the preparation of carbon spheres. Firstly, glucose was dissolved in deionized water. The concentration of glucose solution was 0.2 mol/L. Subsequently, the prepared solution was sealed in Teflon autoclaves and heated by a microwave accelerated reaction system (MARS-10, SINEO) for 120 min at 200 °C. After hydrothermal reaction, the brown precipitates were collected, washed with deionized water and anhydrous alcohol three times, dried at 80 °C for 2 h. Finally, the precipitates were collected for the fabrication of SiC hollow spheres.

2.2. Synthesis of SiC hollow spheres

Firstly, the prepared carbon spheres were dispersed in alcohol to prepare a carbon spheres slurry. Graphite papers with a thickness of 0.5 mm were dipped in the carbon spheres slurry and dried at 50 °C for 1 h. Then, the graphite papers were put into a corundum crucible with the SiO_2 and Si mixture powders, as illustrated in Fig. 1. The molar ratio of the Si and SiO_2 was about 1:2. Subsequently, the assembled crucibles were placed in vacuum sintering furnace, heated to 1450 °C and held for 30 min. The furnace vacuum maintained 10 Pa in the heating process. Finally, the reacted graphite papers were immerged in water and dispersed under the ultrasonic wave. The precipitates were collected and calcined at 500 °C for 2 h to remove the residual carbon.

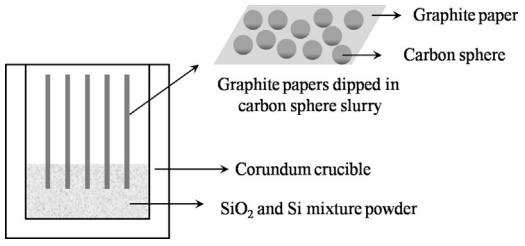

Fig. 1. Illustration of the assembly for the synthesis of SiC hollow spheres.

2.3. Characterization of SiC hollow spheres

X-Ray diffraction (XRD) patterns were obtained on an X-ray diffractometer (D/max-2000, Rigaku) using Cu-Kα radiation. Morphologies of the SiC hollow spheres were observed using scanning electron microscopy (4800S, Hitachi). Transmission electron microscopy (TEM) images were obtained on a Tecnai F30G2 instrument at an accelerating voltage at 200 kV. UV–vis absorption spectra were recorded on a LAMBDA 950UV/Vis/NIR Spectrophotometer. The Brunauer–Emmet–Teller (BET) surface area of the SiC hollow spheres was analyzed by using a nitrogen adsorption apparatus (3H-2000PS4, Beishide). Prior to the nitrogen adsorption measurements, the samples were degassed at 120 °C for 1 h. Pore size distributions were determined from the nitrogen desorption isotherms using the Barrett–Joyner–Halenda (BJH) method.

2.4. Sorption studies

Methylene blue (MB) was dissolved in deionized water to prepare a stock solution with a concentration of 1×10^{-5} mol/L. The solutions for adsorption tests were prepared by loading the catalysts varied from 0.2 to 1.0 g/L. The suspension of MB with SiC hollow spheres was magnetically stirred in dark for 60 min until an adsorption–desorption equilibrium was achieved. Then, samples were taken and centrifuged at 4000 rpm for 10 min. The concentration of the residual MB was measured using a UV–vis spectrophotometer (UV-2600, UNICO) at 664 nm wavelength. These dates were used to calculate the adsorption capacity of the adsorbent. The amount of dye adsorbed (q_e) and efficiency ($\eta\%$) of SiC hollow spheres were calculated by the following equations [21]:

$$q_e = (C_0 - C_e) \times \frac{V}{M} \quad (1)$$

$$\eta\% = \frac{C_0 - C_e}{C_0} \times 100\% \quad (2)$$

where C_0 and C_e are the initial and equilibrium concentrations of dye (mg/L), M is the mass of SiC hollow spheres (g), and V is the volume of solution (L).

2.5. Visible-light photocatalytic activity

Photocatalytic activity of the catalysts was evaluated by degradation of 1×10^{-5} mol/L MB aqueous solution. The loading concentration of the catalysts was varied from 0.2 to 0.8 g/L. Before illumination, the suspension of MB with catalysts was magnetically stirred in dark for 60 min until an adsorption–desorption equilibrium was achieved. Photocatalytic experiments were carried out under a 1000 W Xe lamp with a 420 nm cutoff filter. The photocatalytic device equipped with a cold trap and an air conditioning system, which can control the temperature of the catalytic system. The temperature of the MB solution with catalysts maintained 30 ± 3 °C during the photocatalytic test. At given intervals, a certain amount of

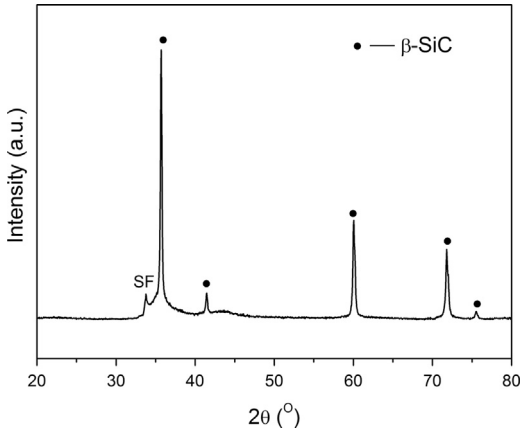

Fig. 2. XRD patterns of the SiC hollow spheres.

the suspension was sampled and centrifuged. MB in the supernatant was measured by UV–vis spectrophotometer at 664 nm wavelength.

3. Results and discussion

3.1. Phase analysis

The powder XRD pattern was used to verify the phase composition of the product, as shown in Fig. 2. It indicates that the products are the mainly face-centered cubic SiC. The peaks at approximately 35.8, 41.3, 60.0, 72.0 and 75.4° correspond to (111), (200), (220), (311), and (222) peaks of β-SiC, which agree with the standard value for β-SiC (JCPDS Card No. 0029-1129). The diffraction peak of 33.5° marked as SF is due to stacking faults in β-SiC [22]. Generally, there are many stacking faults in β-SiC when the particle size is small. The stacking fault density is dependent on the crystallite size of nanostructured SiC [23]. According to the equation of stacking fault density [22,23], the calculated stacking fault density of the obtained β-SiC is about 0.99, which indicates that the crystallite size of the SiC is very small. The crystallite size of the prepared SiC is about 8 nm, which is calculated from the Scherrer equation [24]. Stacking faults are an important type of crystallographic defect, which can be a center for carriers generation and recombination [25]. The high density stacking fault can provide the high density of electron–hole pair, which has a great effect on the photocatalytic properties [3].

3.2. Morphology of the SiC hollow sphere

The morphologies and microstructures of the starting carbon spheres and the prepared SiC hollow spheres are shown in Fig. 3. As shown in Fig. 3(a), the carbon spheres have a uniform size of 200–300 nm, which is similar to the reported colloidal carbon spheres derived from glucose by hydrothermal process [26]. The clearer surface structure of the carbon spheres is revealed by the magnified FESEM image as shown in Fig. 3(b). Individual particulates about 5–10 nm in diameter can be clearly distinguished and these distinguishable spherical particulates appears to be fused together. Fig. 3(c) shows a TEM image of a carbon spheres with a size of about 250 nm. HRTEM image (Fig. 3(d)) shows that the carbon spheres are of highly disorder carbon, which is indicated the spheres consist of amorphous carbon. Fig. 3(e) shows a SEM image of the prepared SiC hollow spheres. The hollow spheres exhibit a uniform size of 200–300 nm, which is similar to the carbon spheres. It implies that the transformation from carbon to SiC maintains the original carbon spheres and presents a shape memory. Moreover, some broken SiC spheres can be found in Fig. 3(e), which indicates the obviously hollow structure. The surface of the SiC hollow spheres is coarse and assembled by SiC nanocystals with a size of 10–30 nm, as shown in Fig. 3(f). Fig. 3(g) shows a TEM image of the SiC hollow spheres. It can be seen that the prepared SiC exhibits a pale region in the center in contrast to dark edges, indicating that the crystals are hollow spheres. The SiC hollow spherical nanocrystals have a uniform shell thickness of 40–60 nm. The HRTEM image of the hollow shell part (Fig. 3(h)) confirms the multi-crystalline structure. Moreover, an amorphous layer with a thickness of 5 nm can be found in the surface of the hollow shell, which might be the SiO_2 formed in the sintering and calcination process.

3.3. BET of the SiC hollow sphere

Fig. 4(a) shows the N_2 adsorption–desorption isotherms of SiC hollow spheres. The isotherms corresponding to the SiC hollow spheres were of type IV, according to Brunauer–Deming–Deming–Teller classification. The adsorption and desorption isotherms become abrupt changes when the relative pressure is in the range from 0.4 to 0.9, which is an outstanding feature of mesoporous materials [27,28]. The hysteresis loop also suggests that the SiC hollow spheres possess a mesoporous structure. The hysteresis loop at lower relative pressure ranges ($0.4 < P/P_0 < 0.9$) is associated with finer intra-aggregated pores within primary agglomerated particles, while that at higher relative pressure ranges ($0.9 < P/P_0 < 1$) is related to larger inter-aggregated pores between secondary aggregated particles [28]. The BET report showed that the sample has a high surface area of 83.5 m^2/g and a large pore volume of 0.43 cm^3/g. The BJH method was employed to calculate the pore size distribution of the sample, and the result was shown in Fig. 4(b). The sample shows bimodal pore size distribution ranged from 2 to 40 nm. The sample contains small mesopores (c.a. 10.1 nm) and larger mesopores with a maximum pore diameter of c.a. 24.9 nm. The smaller mesopores is related to finer intra-aggregated pores formed between primary particles, and larger mesopores is associated with larger inter-aggregated pores produced by inter-aggregated secondary particles [29].

3.4. Absorption spectrum of the SiC hollow sphere

Fig. 5 shows the UV–vis diffusion reflectance spectra of the SiC hollow sphere. The absorbance of SiC hollow spheres is mainly ranged from 300 to 800 nm and increase monotonically with the wavelength. It is indicated that the photo-response of

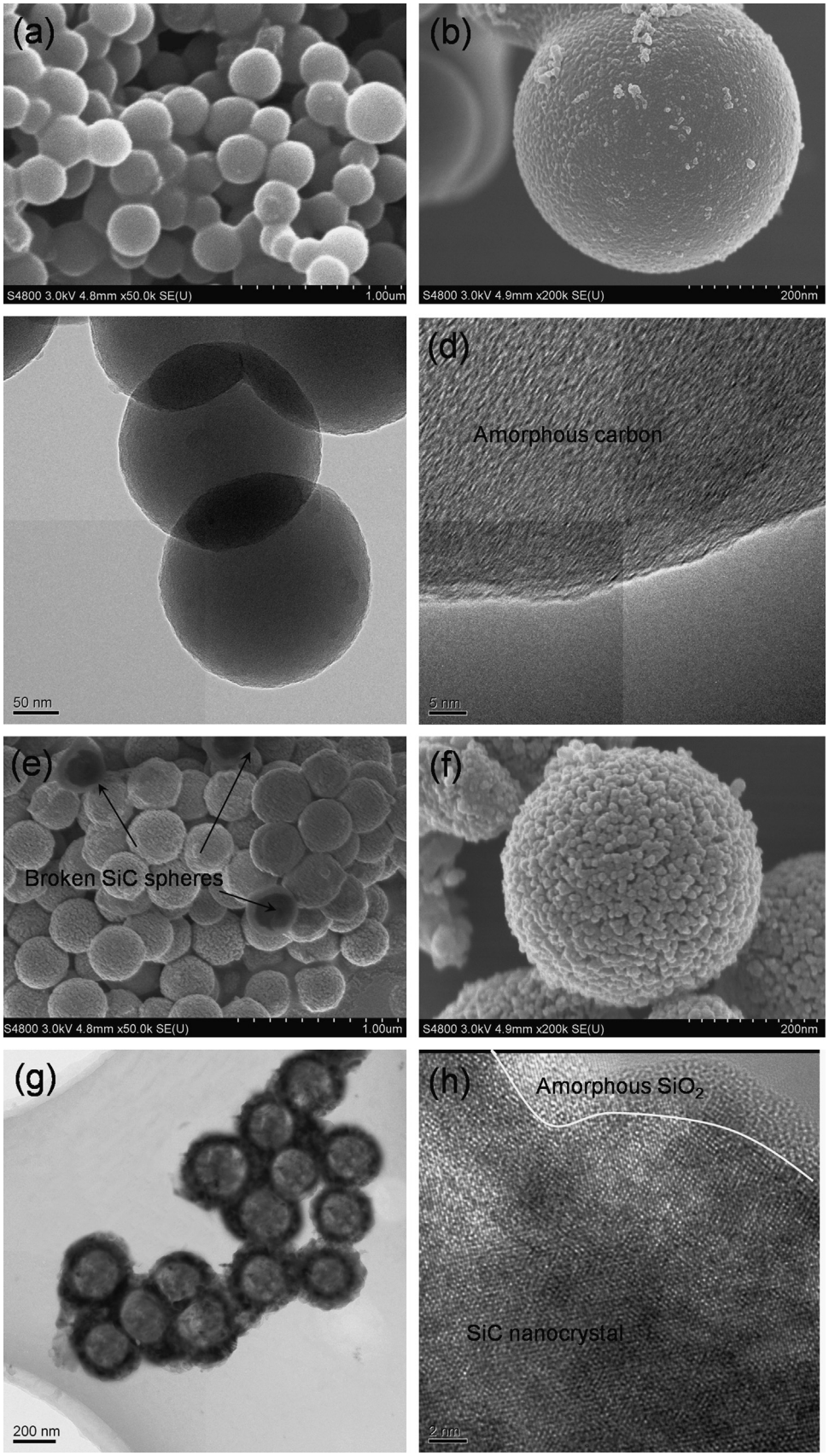

Fig. 3. Morphologies and microstructures of the starting carbon spheres and the prepared SiC hollow spheres: (a) and (b) SEM image of the staring carbon spheres, (c) and (d) TEM image of the carbon spheres; (e) and (f) SEM image of the prepared SiC hollow spheres, (g) and (h) TEM image of the SiC hollow spheres.

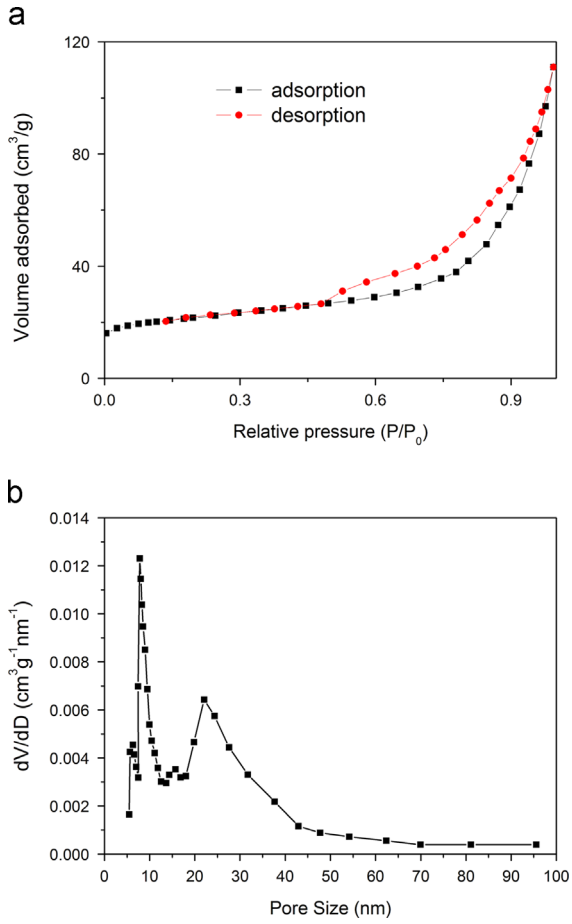

Fig. 4. Nitrogen adsorption–desorption isotherm (a) and pore size distribution and (b) curves of SiC hollow spheres.

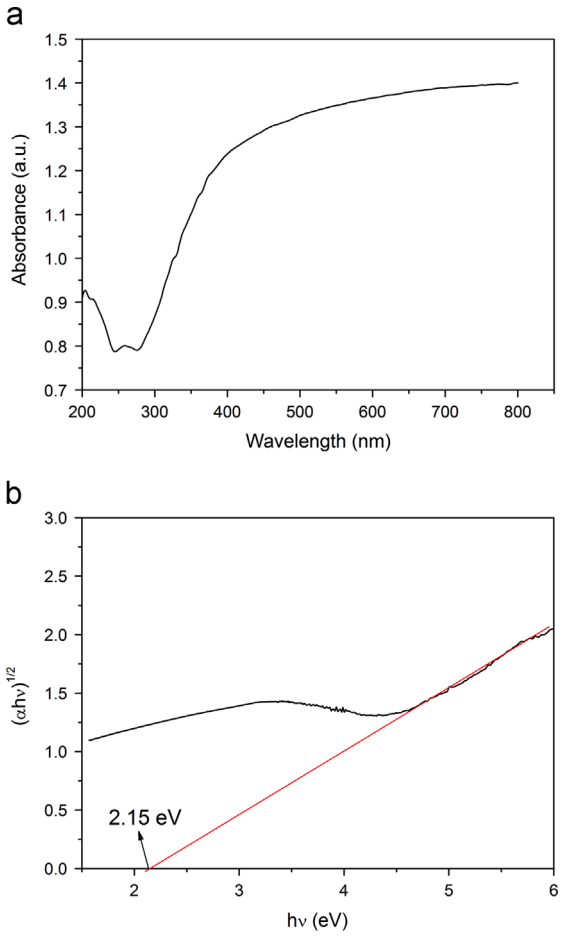

Fig. 5. UV–vis diffusion reflectance spectra (a) and the corresponding plots of $(\alpha h\nu)^{1/2}$ versus hν for the SiC hollow spheres.

the SiC hollow spheres can expand to visible-light region with a high absorbance. The UV–vis diffusion reflectance results show that the SiC hollow spheres are potential for the solar-energy application. In order to calculate the band gap of the SiC samples, the K–M model is employed for treating the absorption data of the samples [11]. Fig. 5(b) present the indirect band gap energy estimated from a plot of $(\alpha h\nu)^{1/2}$ versus photo energy (hν) according to the K–M model. The estimated band gap energy of SiC hollow spheres is 2.15 eV, which is lower than that of the commonly known bulk 3C–SiC (2.39 eV) due to stacking faults in the SiC hollow spheres.

3.5. Absorption behavior of the SiC hollow spheres

Fig. 6(a) shows changes in the absorption spectra of MB aqueous solution loading with various concentrations of SiC hollow spheres. The absorption peaks at 664 nm drops gradually with the increasing of SiC hollow spheres concentration. The peak almost disappears after loading with 1.0 g/L SiC hollow spheres, exhibiting excellent adsorption capacity. It was observed that the adsorption capacity decreases from 13.6 to 9.5 mg/g with the increase of the loading amount of SiC hollow spheres, as shown in Fig. 6(b). On the other hand, the removal efficiency increases from 27.2% to 94.6% as the SiC hollow spheres concentration increases from 0.2 to 1.0 g/L. This can be attributed to the increase of the adsorbent specific surface area and availability of more adsorption sites. Consequently, the loading concentration of the SiC hollow spheres was control at 0.2, 0.4, 0.6 and 0.8 g/L in the subsequent experiments to investigate the photocatalytic activity of SiC hollow spheres.

3.6. Visible-light photocatalytic activity

In order to demonstrate the potential environmental application for the removal of contaminants from water, we investigated the visible-light photocatalytic activities of the SiC hollow spheres using photocatalytic degradation of MB as a test reaction. Fig. 7 shows the photocatalytic degradation of MB in the presence of different concentrations of SiC hollow spheres under visible-light illumination. The blank experiment without catalysts is also investigated. The value can be neglected with about 5% of conversion after 480 min illumination. A period of adsorption in the dark of 60 min has been chosen to obtain adsorption–desorption equilibrium. Then, the concentration of MB drops gradually with increasing irradiation time and almost disappears. The degradation efficiency increases with the increasing of SiC hollow spheres concentration. When the SiC hollow spheres concentration is 0.8 g/L,

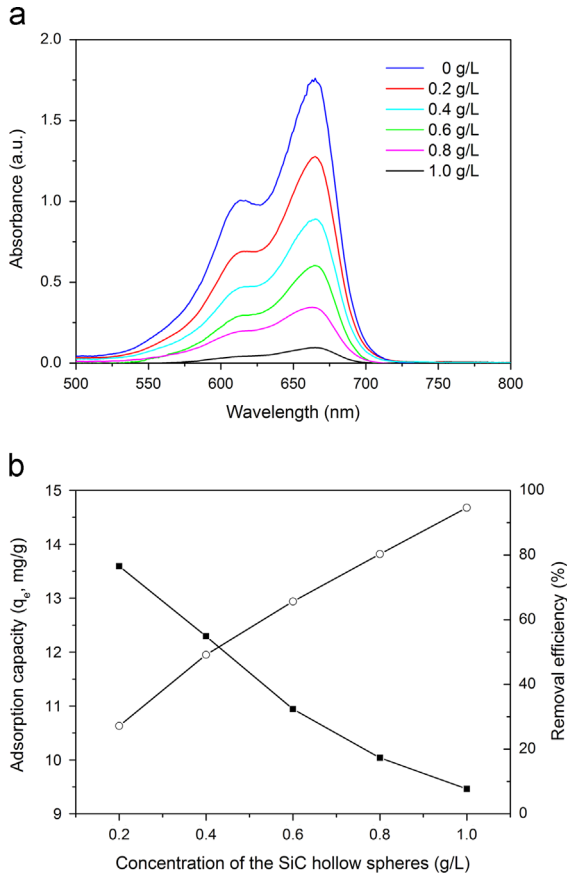

Fig. 6. (a) Adsorption changes of the MB aqueous solution in the presence of varied concentration of SiC hollow spheres and (b) Effect of SiC hollow spheres concentration on the adsorption capacity and removal efficiency of MB.

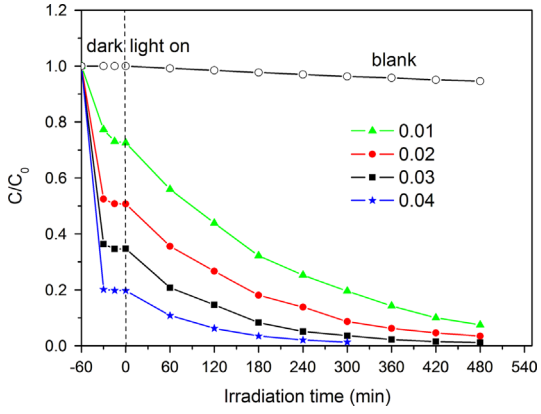

Fig. 7. Photocatalytic degradation of MB in the presence of different concentrations of SiC hollow spheres under visible-light illumination.

the MB is almost completely degraded after 300 min visible-light illumination. It is known that the degradation of MB by photocatalysis is heterogeneous catalysis reaction [30,31]. The Langmuir-Hinshelwood model can be used to describe the heterogeneous photocatalytic reaction. The photocatalytic degradation of MB obeys apparently pseudo-first order kinetics at low initial insecticide concentration and the rate expression is given by Eq. (3) [32].

$$\ln(C_0/C_t) = K_{aps}t \quad (3)$$

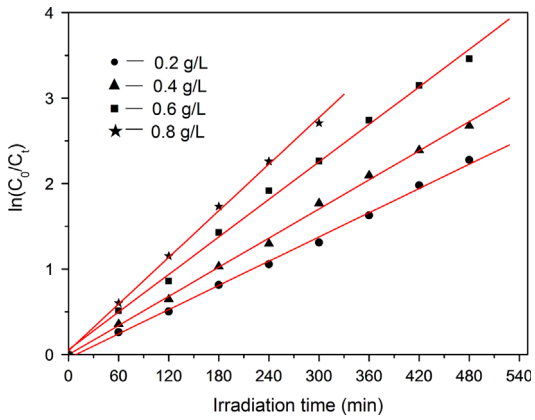

Fig. 8. Plot of $\ln(C_0/C_t)$ versus t in the presence of different concentrations of SiC hollow spheres under visible-light illumination.

where, k_{aps} is the apparent pseudo-first-order rate constant, C_0 is the initial equilibrium concentration of MB; C_t is the concentration of MB remaining in the solution after t min visible-light illumination.

Fig. 8 show plot of $\ln(C_0/C_t)$ versus irradiation time (t) for the degradation of MB in the presence of different concentrations of SiC hollow spheres under visible-light illumination. As it is clear from these figures, removal of the dye concentration obeys a linear pattern coordinated with good precision. This means that the pseudo-first order kinetic of dye removal kinetic is acceptable for the degradation of MB in the presence of SiC hollow spheres under visible-light illumination. The data of k_{app} and correlation coefficient R^2 are listed in Table 1. Comparison of the dates of k_{app} show that the rate of degradation increases with the increasing of the SiC hollow spheres concentration.

It is known that catalyst dosage is an important parameter that can affect the degradation rate in photocatalytic processes. The prepared SiC hollow spheres are mesoporous materials with high surface area. Usually, a large surface area can offer more active adsorption sites and photocatalytic reaction centers. Furthermore, the prepared SiC hollow spheres present the enhanced light-absorption and extended light-response range, which results in a significant increase of light-harvesting. In additionally, the prepared SiC hollow spheres exhibits the lower band gap energy, which is of benefit to the generation of excited electrons and holes. The number of excited electrons and holes created by light irradiation plays an important role in affecting the photocatalytic efficiency. The higher the number of carriers has, the better the photocatalyst is. Thus, the enhanced photocatalytic activity of SiC hollow spheres can be attributed to their high surface area as well as large light-harvesting efficiencies.

4. Conclusion

In summary, SiC hollow spheres have been successfully synthesized by the reaction of carbon spheres and silicon monoxide vapor. The diameter of SiC hollow spheres is about 300 nm and the shell thickness is about 50 nm. The transformation from carbon to SiC maintains the original carbon

Table 1
Pseudo-first order apparent constant values for the degradation of MB in the presence of different concentrations of SiC hollow spheres under visible-light illumination.

Concentrations of SiC hollow spheres (g/L)	k_{app} (min^{-1})	R^2
0.2	0.00473	0.99863
0.4	0.00589	0.99925
0.6	0.00732	0.99838
0.8	0.00909	0.99902

spheres and presents a shape memory. The SiC hollow spheres have a high surface area of 83.5 m^2/g and exhibit a mesoporous structure. The photo-response of the SiC hollow spheres can expand to visible-light region with band gap energy of 2.15 eV. The photodegradation rate of MB reaches approximately 98% after 300 min of visible-light irradiation. The SiC hollow spheres exhibit a significantly enhanced photocatalytic activity due to their high surface area as well as large light-harvesting efficiencies. This approach provides a simple and economical method to synthesize uniform SiC hollow spheres with high photocatalytic activity.

Acknowledgments

This work has been supported by the National Natural Science Foundation of China (Grant no. 51302160), Innovation Team Assistance Foundation of Shaanxi Province (Grant no. 2013KCT-06), the China Postdoctoral Science Foundation (Grant no. 2013M530414), and the Natural Science Foundation of Education Department of Shaanxi Provincial (Grant no. 2013JK0938). The project T201207 was supported by the Shenzhen Key Laboratory of Special Functional Materials.

References

[1] J.M. Herrmann, Heterogeneous photocatalysis: state of the art and present applications, Topics Catal. 34 (2005) 49–65.
[2] D. Bahnemann, Photocatalytic water treatment: solar energy applications, Solar Energy 77 (2004) 445–459.
[3] H. Tong, S. Ouyang, Y.P. Bi, N. Umezawa, M. Oshikiri, J.H. Ye, Nano-photocatalytic materials: possibilities and challenges, Adv. Mater. 24 (2012) 229–251.
[4] A. Kubacka, M. Fernández-García, G. Colón, Advanced nanoarchitectures for solar photocatalytic applications, Chem. Rev. 112 (2012) 1555–1614.
[5] K. Zekentes, K. Rogdakis, SiC nanowires: material and devices, J. Phys. D: Appl. Phys 44 (2011) 133001.
[6] P. Nguyen, C. Pham, Innovative porous SiC-based materials: from nanoscopic understandings to tunable carriers serving catalytic needs, Appl. Catal. A-Gen. 391 (2011) 443–454.
[7] J.Y. Fan, X.L. Wu, P.K. Chu, Low-dimensional SiC nanostructures: fabrication, luminescence, and electrical properties, Prog. Mater. Sci. 51 (2006) 983–1031.
[8] R.B. Wu, L.L. Wu, G.Y. Yang, Y. Pan, J.J. Chen, R. Zhai, Fabrication and photoluminescence of bicrystalline SiC nanobelts, J. Phys. D: Appl. Phys 40 (2007) 3697–3701.
[9] W.M. Zhou, X. Liu, Y.F. Zhang, Simple approach to β-SiC nanowires: synthesis, optical, and electrical properties, Appl. Phys. Lett. 89 (2006) 223124.
[10] H.K. Seong, H.J. Choi, S.K. Lee, J.I. Lee, D.J. Choi, Optical and electrical transport properties in silicon carbide nanowires, Appl. Phys. Lett. 85 (2004) 1256–1258.
[11] W.M. Zhou, L.J. Yan, Y. Wang, Y.F. Zhang, SiC nanowires: a photocatalytic nanomaterial, Appl. Phys. Lett. 89 (2006) 013105.
[12] H.L. Liu, G.W. She, L.X. Mu, W.S. Shi, Porous SiC nanowire arrays as stable photocatalyst for water splitting under UV Irradiation, Mater. Res. Bull. 47 (2012) 917–920.
[13] C. He, X. Wu, J. Shen, P.K. Chu, High-efficiency electrochemical hydrogen evolution based on surface autocatalytic effect of ultrathin 3C–SiC nanocrystals, Nano Lett. 12 (2012) 1545–1548.
[14] J.Y. Hao, Y.Y. Wang, X.L. Tong, G.Q. Jin, X.Y. Guo, Photocatalytic hydrogen production over modified SiC nanowires under visible light irradiation, Int. J. Hydrog. Energ. 37 (2012) 15038–15044.
[15] X.W. Lou, L.A. Archer, Z.C. Yang, Hollow micro-/nanostructures: synthesis and applications, Adv. Mater. 20 (2008) 3987–4019.
[16] J. Hu, M. Chen, X. Fang, L.M. Wu, Fabrication and application of inorganic hollow spheres, Chem. Soc. Rev. 40 (2011) 5472–5491.
[17] Y. Kondo, H. Yoshikawa, K. Awaga, M. Murayama, T. Mori, K. Sunada, et al., Preparation, photocatalytic activities, and dye-sensitized solar-cell performance of submicron-scale TiO_2 hollow spheres, Langmuir 24 (2008) 547–550.
[18] Z.Y. Liu, L.J. Ci, N.Y. Jin-Phillipp, M. Riihle, Vapor–solid reaction for silicon carbide hollow spherical nanocrystals, J. Phys. Chem. C 111 (2007) 12517–12521.
[19] K. Wang, H.T. Wang, Y.B. Cheng, Synthesis of nanostructured silicon carbide spheres from mesoporous C–SiO_2 nanocomposites, Chem. Commun. 46 (2010) 303–305.
[20] P. Li, L.Q. Xu, Y.T. Qian, Selective Synthesis of 3C–SiC Hollow Nanospheres and Nanowires, Cryst. Growth Des. 8 (2008) 2431–2436.
[21] M. Iram, C. Guo, Y. Guan, A. Ishfaq, H. Liu, Adsorption and magnetic removal of neutral red dye from aqueous solution using Fe_3O_4 hollow nanospheres, J. Hazard. Mater. 181 (2010) 1039–1050.
[22] W.S. Seo, K. Koumoto, Stacking faults in β-SiC formed during carbothermal reduction of SiO_2, J. Am. Ceram. Soc. 79 (1996) 1777–1782.
[23] W.S. Seo, K. Koumoto, Effects of Boron, carbon, and iron content on the stacking fault formation during synthesis of b-SiC particles in the system SiO_2-C–H_2, J. Am. Ceram. Soc. 81 (1998) 1255–1261.
[24] Y. Xu, L. Cheng, L. Zhang, W. Zhou, Morphology and growth mechanism of silicon carbide chemical vapor deposited at low temperatures and normal atmosphere, J. Mater. Sci. 34 (1999) 551–555.
[25] S.G. Sridhara, F.H.C. Carlsson, J.P. Bergman, E. Janzén, Luminescence from stacking faults in 4H SiC, Appl. Phys. Lett. 79 (2001) 3944–3946.
[26] Y. Mi, W. Hu, Y. Dan, Y. Liu, Synthesis of carbon micro-spheres by a glucose hydrothermal method, Mater. Lett. 62 (2008) 1194–1196.
[27] D. Chen, F. Huang, Y.B. Cheng, R.A. Caruso, Mesoporous anatase TiO_2 beads with high surface areas and controllable pore sizes: a superior candidate for high-performance dye-sensitized solar cells, Adv. Mater. 21 (2009) 2206–2210.
[28] Z. Teng, Y. Han, J. Li, F. Yan, W. Yang, Preparation of hollow mesoporous silica spheres by a sol–gel/emulsion approach, Micropor. Mesopor. Mat. 127 (2010) 67–72.
[29] L. Zhao, J. Li, Y. Shi, S. Wang, J. Hu, B. Dong, H. Lu, P. Wang, Double light-scattering layer film based on TiO_2 hollow spheres and TiO_2 nanosheets: improved efficiency in dye-sensitized solar cells, J. Alloy. Compd. 575 (2013) 168–173.
[30] Z. Yu, S. Chuang, Probing methylene blue photocatalytic degradation by adsorbed ethanol with in situ IR, J. Phys. Chem. C 111 (2007) 13813–13820.
[31] A. Houas, H. Lachheb, M. Ksibi, E. Elaloui, C. Guillard, J.M. Herrmann, Photocatalytic degradation pathway of methylene blue in water, Appl. Catal. B-Environ. 31 (2001) 145–157.
[32] K. Lv, J. Li, X. Qing, W. Li, Q. Chen, Synthesis and photo-degradation application of WO_3/TiO_2 hollow spheres, J. Hazard. Mater. 189 (2011) 329–335.